

EMBRIDGE: ENHANCING GESTURE GENERALIZATION FROM EMG SIGNALS THROUGH CROSS-MODAL REPRESENTATION LEARNING

006 **Anonymous authors**

007 Paper under double-blind review

ABSTRACT

013 Hand gesture classification using high-quality structured data such as videos, im-
 014 ages, and hand skeletons is a well-explored problem in computer vision. Alterna-
 015 tively, leveraging low-power, cost-effective bio-signals, e.g. surface electromyo-
 016 graphy (sEMG), allows for continuous gesture prediction on wearable devices.
 017 In this work, we aim to enhance EMG representation quality by aligning it with
 018 embeddings obtained from structured, high-quality modalities that provide richer
 019 semantic guidance, ultimately enabling zero-shot gesture generalization. Specif-
 020 ically, we propose EMBridge, a cross-modal representation learning framework
 021 that bridges the modality gap between EMG and pose. EMBridge learns high-
 022 quality EMG representations by introducing a Querying Transformer (Q-Former),
 023 a masked pose reconstruction loss, and a community-aware soft contrastive learn-
 024 ing objective that aligns the relative geometry of the embedding spaces. We eval-
 025 uate EMBridge on both in-distribution and unseen gesture classification tasks and
 026 demonstrate consistent performance gains over all baselines. To the best of our
 027 knowledge, EMBridge is the first cross-modal representation learning framework
 028 to achieve zero-shot gesture classification from wearable EMG signals, showing
 029 potential toward real-world gesture recognition on wearable devices.

1 INTRODUCTION

030 Hand gesture recognition on wearable devices has recently attracted significant interest (Pyun et al.,
 031 2024; Moin et al., 2021) and demonstrated potential across diverse applications such as rehabil-
 032 itation (Marcos-Antón et al., 2023), human-computer interaction (Jarque-Bou et al., 2021), and
 033 prosthetic control (Yu et al., 2023). With advances in deep learning and the availability of large-
 034 scale visual data, including videos and motion capture (Casile et al., 2023), vision-based models
 035 have achieved remarkable success (Pavlakos et al., 2023; Qi et al., 2024). However, cameras suffer
 036 from high power demands and privacy concerns, and potential occlusions can destabilize vision-
 037 based classification. This has motivated growing interest in low-power, easily integrable sensors
 038 (Tchantchane et al., 2023), such as surface electromyography (sEMG), for gesture recognition on
 039 wearable devices (Tchantchane et al., 2023; Wang et al., 2023). Deep learning approaches have been
 040 explored for EMG-based gesture classification, including convolutional neural networks (CNNs)
 041 (Atzori et al., 2016), recurrent neural networks (RNNs) (Liu et al., 2021), and Transformers (Mon-
 042 tazerin et al., 2023). However, predicting hand gestures from wearable EMG, especially generaliz-
 043 ing to unseen gestures without task-specific training, remains challenging (Laput & Harrison, 2019).
 044 This is mainly because of the high variability and fine dexterity of human hand movements, sensor
 045 noise, and/or the limited scale of publicly available data (Lee et al., 2024a; Pereira et al., 2024;
 046 Tam et al., 2024). Due to the noisy and heterogeneous nature of EMG signals, learning from EMG
 047 alone (through self-supervised learning or supervised end-to-end training) may not reliably yield
 048 generalizable and discriminative representations (later demonstrated in our experiments).

049 An effective strategy to overcome the above limitations is to leverage another modality that offers
 050 richer semantic structure and higher signal quality as guidance during representation learning. This
 051 can be achieved through cross-modal representation learning, which has proven highly effective
 052 in improving the quality of learned embeddings and shown remarkable success in vision-language
 053 models (Xie et al., 2025; Li et al., 2023), audio-visual language models (Gurram et al., 2022; Guo

054 et al., 2025), and in biosignals such as IMU-video-text alignment (Moon et al., 2022) and EEG-text
 055 alignment (Feng et al., 2023). However, aligning representations across modalities has not yet been
 056 fully explored for wearable EMG signals. Given paired EMG recordings and kinematic hand pose
 057 annotations collected simultaneously, we can study cross-modal alignment between EMG and pose.
 058 **Unlike visual data, pose data directly captures the kinematics of hand movements, making it an**
 059 **informative modality for guiding EMG representation learning.** Therefore, we introduce a cross-
 060 modal framework for EMG representation learning that leverages a high-quality anchor modality,
 061 where structured pose data provides richer supervisory signals by capturing structural and semantic
 062 relationships. Our goal is to improve the quality of EMG embeddings, enabling generalization to
 063 new users and unseen gestures at test time without the need for additional training or large-scale data
 064 collection. **The potential practical application of our framework can be wearable Human-Computer**
 065 **Interaction. In scenarios like VR/AR and prosthetic control applications (Jarque-Bou et al., 2021;**
 066 **Yu et al., 2023), a wrist-worn device must continuously infer hand gestures from EMG signals to**
 067 **drive a virtual avatar or robotic hand. A critical bottleneck is that users cannot be expected to record**
 068 **training data for every possible movement they might perform. Our framework is designed to enable**
 069 **zero-shot generalization, allowing the system to recognize novel gestures without requiring the user**
 070 **to provide training samples.**

071 We first introduce two unimodal encoders trained separately on EMG and pose data, and then align
 072 their output embeddings. Unlike classical approaches such as CLIP or BLIP (Radford et al., 2021;
 073 Li et al., 2023; 2022), which symmetrically update both encoders toward a shared latent space,
 074 our design adopts an asymmetric setup, where the pose encoder is frozen as an anchor and only
 075 the EMG encoder is optimized. On this basis, we propose **EMBridge**, a cross-modal representa-
 076 tion learning framework that bridges the modality gap between EMG and pose and enhances the
 077 representation quality learned from EMG signals through advanced alignment with pose representa-
 078 tions. EMBridge consists of three components: a Querying Transformer (Q-former) (Li et al., 2023)
 079 that extracts pose-informative queries and aligns EMG and pose, a masked pose reconstruction loss
 080 (MPRL) that encourages queries to carry structured pose information, and a community-aware soft
 081 contrastive learning (CASCLe) objective that considers the neighborhood structures of poses and
 082 aligns the relative geometry in the latent space across modalities. **Standard contrastive learning**
 083 **approaches (e.g., InfoNCE) treat all non-matching samples as equally distant negatives. However,**
 084 **this assumption is suboptimal for our pose data, which is inherently continuous. And poses across**
 085 **different gesture categories can be semantically close. To capture these structural similarities and**
 086 **avoid confusing the model with hard negatives, we introduce CASCLe, which utilizes geometric**
 087 **proximity in the pose space to generate soft targets.** Together, these objectives guide the EMG
 088 encoder to capture pose-relevant semantics and produce discriminative, generalizable embeddings.
 089 Unlike general-purpose multi-modal alignment, EMBridge is designed as a specialized solution for
 090 EMG-based gesture classification through cross-modal supervision.

091 We utilize large-scale public EMG datasets (Salter et al., 2024; Atzori et al., 2014), which pro-
 092 vides simultaneous paired EMG and pose recordings to pre-train our EMBridge model and perform
 093 downstream evaluations. We design a gesture classification task to evaluate EMG representation
 094 quality. Following CLIP evaluation protocol (Radford et al., 2021), we validate the learned EMG
 095 representations through zero-shot classification and linear probing, demonstrating superior perfor-
 096 mance on both in-distribution and unseen gestures compared to benchmark models. In summary,
 097 our contributions are two-fold:

- 098 • We propose a cross-modal representation learning strategy to enhance the quality of EMG
 099 representations learned from noisy EMG signals by aligning them with high-quality pose
 100 representations.
- 101 • To the best of our knowledge, EMBridge is the first cross-modal framework enabling zero-
 102 shot classification of unseen gestures for EMG signals from wearable devices.

103 2 METHODOLOGY

104 2.1 PRELIMINARIES

105 **Definition 1. EMG, pose data, and gesture classes.** Let $\mathcal{X} = \{\mathbf{x}_i \in \mathbb{R}^{C \times T}\}_{i=1}^N$ denote multi-
 106 channel EMG sequences with C channels and window length T , and let $\mathcal{P} = \{\mathbf{p}_i \in \mathbb{R}^{J \times T}\}_{i=1}^N$

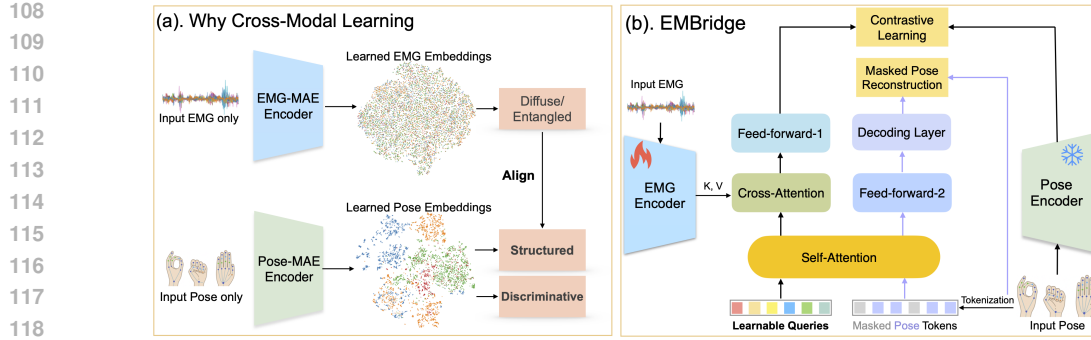


Figure 1: (a) Motivation for cross-modal representation learning: using the same MAE pre-training, pose embeddings are semantically structured and well-separated across gestures (colors), whereas EMG embeddings are not. This motivates leveraging pose as guidance to structure the EMG representation space. (b) Detailed architecture of EMBridge. Only one transformer block (self-attention, cross-attention, and feed-forward layers) is shown for clarity, the model uses four such blocks.

denote the paired pose sequences of joint angles, where J is the number of joints in a predefined hand skeleton (Salter et al., 2024). Here, N is the total number of paired samples. We define a pose as the instantaneous state of the hand skeleton (20 joint angles) at a single time point, whereas a gesture is a temporal sequence of poses over a time window. Let $\mathcal{Y} = \{1, \dots, K\}$ denote the gesture classes, and let $\{y_i\}_{i=1}^N$ be the labels with $y_i \in \mathcal{Y}$. Each pose \mathbf{p}_i has a unique label y_i , although multiple samples may share the same label. The paired dataset is

$$\mathcal{D} = \{(\mathbf{x}_i, \mathbf{p}_i, y_i)\}_{i=1}^N,$$

which we split into \mathcal{D}_{tr} , \mathcal{D}_{val} , and $\mathcal{D}_{\text{test}}$. Let $\mathcal{Y}_{\text{in}} \subset \mathcal{Y}$ be the in-distribution gesture classes and $\mathcal{Y}_{\text{unseen}} \subset \mathcal{Y}$ be the unseen gesture classes, with $\mathcal{Y}_{\text{in}} \cap \mathcal{Y}_{\text{unseen}} = \emptyset$. For subset $S \in \{\text{tr, val, test}\}$,

$$\mathcal{D}_S^{\text{in}} = \{(\mathbf{x}, \mathbf{p}, y) \in \mathcal{D}_S : y \in \mathcal{Y}_{\text{in}}\}, \quad \mathcal{D}_S^{\text{unseen}} = \{(\mathbf{x}, \mathbf{p}, y) \in \mathcal{D}_S : y \in \mathcal{Y}_{\text{unseen}}\}.$$

Definition 2. Unimodal Encoders. Let \mathcal{E}_x and \mathcal{E}_p map EMG and pose, respectively, into \mathbb{R}^d . When the pose encoder is used frozen, we write \mathcal{E}_p^* .

Unimodal Encoder Pre-training. We adopt a Transformer encoder (Vaswani et al., 2023) with a linear tokenizer to map raw signals into d -dimensional token embeddings. A patch length S along time yields $L = \lfloor T/S \rfloor$ non-overlapping tokens. We flatten channels within each patch and project to $\mathbf{a}_i \in \mathbb{R}^d$. Following masked autoencoders (MAE) (He et al., 2021), we randomly mask a certain ratio of input tokens. The encoder processes only unmasked tokens and the transformer decoder reconstructs all tokens. The reconstruction loss is a mean squared error loss only applied to the masked tokens. We pre-train the EMG and pose encoders independently, yielding \mathcal{E}_x and \mathcal{E}_p . We use a mask ratio of 0.5 and a patch length of $S = 200$. Unlike CLIP, which is trained on billions of image–text pairs, we align strong unimodal encoders to reduce the need for large-scale paired data.

2.2 EMBRIDGE

The proposed cross-modal representation learning framework EMBridge comprises three components: (i) a Querying Transformer that acts as an information bottleneck, extracting pose-informative features from the EMG encoder; (ii) a Masked Pose Reconstruction Loss that strengthens representation learning; and (iii) a Community-Aware Soft Contrastive Learning objective that aligns the relative geometry of the EMG and pose spaces by matching their community-level similarity structures, yielding a more structured EMG latent space. The framework is shown in Figure 1.

2.2.1 QUERYING TRANSFORMER (Q-FORMER).

Inspired by BLIP-2 (Li et al., 2023), we use a set of learnable queries to extract pose-informative features from the EMG encoder. Let $Q^{(0)} \in \mathbb{R}^{M \times d}$ be M learnable queries. The Q-Former F_ϕ

stacks 4 self-attention blocks (each with a feed-forward layer) and 2 cross-attention layers inserted every other block, whose keys/values are from $\mathcal{E}_x(\mathbf{x})$. The self-attention modules of the Q-Former are initialized from the pre-trained Pose-MAE encoder \mathcal{E}_p^* while cross-attention layers are randomly initialized. All Q-Former parameters and the EMG encoder \mathcal{E}_x are trainable, while the pose encoder \mathcal{E}_p^* remains frozen. The Q-Former takes the learnable queries $Q^{(0)}$ as input and produces the same length of queries with learned representations $Q' \in \mathbb{R}^{M \times d}$. We train the Q-Former using a contrastive objective following Li et al. (2022). Given the pose embedding $v_i = \mathcal{E}_p^*(\mathbf{p}_i)$, we select the query token that has the highest cosine similarity with v_i as $u_i = Q'_{m^*(i)}$, $m^*(i) = \arg \max_{m \in \{1, \dots, M\}} \frac{Q'_m^\top v_i}{\|Q'_m\| \|v_i\|}$. Given a mini-batch of size B , we define the softmax over EMG–pose similarities $q_{ij} = \frac{\exp(u_i^\top v_j / \tau)}{\sum_{k=1}^B \exp(u_i^\top v_k / \tau)}$. Let $I \in \{0, 1\}^{B \times B}$ be the one-hot indicator matrix with $I_{ij} = 1$ iff $j = i$ (matching pairs on the diagonal). The Information Noise-Contrastive Estimation (InfoNCE) loss (van den Oord et al., 2019) can then be written as

$$\mathcal{L}_{\text{InfoNCE}} = -\frac{1}{B} \sum_{i=1}^B \sum_{j=1}^B I_{ij} \log q_{ij}. \quad (1)$$

Unlike CLIP, where both encoders are trained jointly, in our setup the pose encoder is frozen and serves as a fixed anchor, **since pose representations are higher-quality and more structured compared to EMG representations**. So we adopt the standard InfoNCE loss (EMG→pose) rather than a symmetric variant, since gradients only flow into the EMG encoder while the pose embeddings remain fixed. By encouraging the learnable queries to extract EMG features that are most consistent with pose representations, the Q-Former efficiently and effectively aligns EMG and pose.

2.2.2 MASKED POSE RECONSTRUCTION LOSS (MPRL)

Beyond the contrastive loss, we add a masked reconstruction objective on input pose tokens to enrich the representation learning process (Li et al., 2023). Specifically, in the first forward pass, the Q-Former produces query embeddings $Q' \in \mathbb{R}^{M \times d}$. In the second forward pass, we concatenate masked pose tokens $\tilde{P} = [\tilde{p}_1, \dots, \tilde{p}_L]$ with Q' and apply the same self-attention modules with an attention mask: pose tokens may attend to all queries, while queries attend only to themselves. Cross-attention from pose tokens to EMG is also disabled, pose cannot directly access EMG features. Thus, the information required to reconstruct masked pose tokens must be captured in Q' , enforcing that queries extract pose-informative content from EMG. Let \mathcal{M} be the set of masked pose-token indices and $H_P = F_\phi([Q; \tilde{P}]) \in \mathbb{R}^{(M+L) \times d}$ denote the outputs of Q-Former. The mask ratio is r . A decoding layer g maps the outputs back to input pose token space. We minimize

$$\mathcal{L}_{\text{MPRL}} = \frac{1}{|\mathcal{M}|} \sum_{m \in \mathcal{M}} \|g(H_P[m]) - P[m]\|_2^2, \quad (2)$$

where $P[m]$ is the ground-truth pose token at index m . Jointly optimizing $\mathcal{L}_{\text{MPRL}}$ with the contrastive loss encourages the Q-Former to learn denoised, pose-informative EMG representations and then yields a EMG latent space with richer pose semantics that can extrapolate to new gestures.

2.2.3 COMMUNITY-AWARE SOFT CONTRASTIVE LEARNING (CASCLE)

We propose CASCLe, which aligns EMG to pose by matching relative geometry of embeddings spaces rather than only instance-level pairs. In standard contrastive learning, all non-matching poses are treated as negatives, even if some are semantically very close to the true positive. This treatment is suboptimal because grouping similar poses as strict negatives confuses the model and leads to unstable gradients. CASCLe addresses this by assigning soft targets. Poses that are more similar to the ground-truth pose receive higher probabilities, while relatively dissimilar ones receive lower or zero probabilities. Since the pose encoder \mathcal{E}_p^* is frozen, its embedding space defines a fixed relational graph. CASCLe builds soft targets from this graph and trains the Q-Former queries to learn similar neighborhood structures for EMG embeddings, which strengthens overall semantic consistency with pose. An illustration of CASCLe is shown in Figure 2.

Pose communities. We cluster pre-trained Pose-MAE embeddings (offline) using k -means (Likas et al., 2003) to obtain N_c centroids $\mathcal{C} \in \mathbb{R}^{N_c \times d}$ (all ℓ_2 -normalized). For a mini-batch of pose

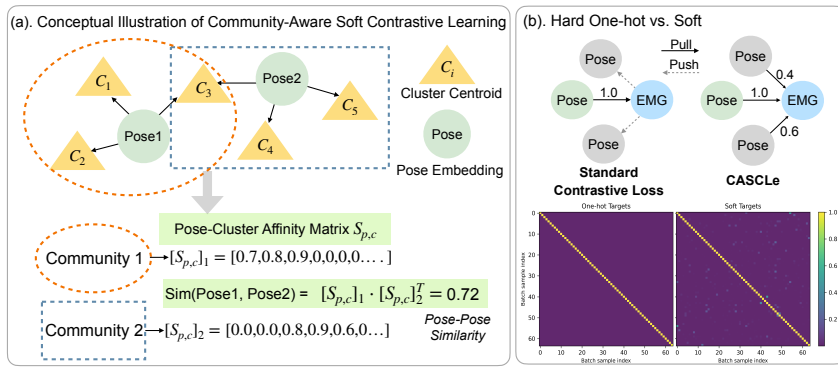


Figure 2: Unlike conventional contrastive loss that relies on one-hot targets, (a). CASCLe constructs soft targets based on community-level similarity. Each community is represented by affinities to cluster centroids, and pose–pose similarity is computed from affinity vectors. Soft targets used in CASCLe are shown in (b), computed from a batch of 64 samples for clearer visualization.

embeddings $P = [v_1; \dots; v_B] \in \mathbb{R}^{B \times d}$, We compute a *pose–cluster affinity matrix* $S_{p,c} = P \mathcal{C}^\top \in \mathbb{R}^{B \times N_c}$, where each row is sparsified by keeping only the top- k_c closest clusters. This keeps the community size reasonable and excludes irrelevant clusters, reducing noise in soft targets.

$$[S_{p,c}]_{ij} \leftarrow \begin{cases} [S_{p,c}]_{ij}, & j \in \text{TopK}(S_{p,c}[i, :]), \\ 0, & \text{otherwise.} \end{cases} \quad (3)$$

Pose–pose similarity matrix. The community-aware pose–pose similarity matrix is then defined as $S_{p,p} = S_{p,c} S_{p,c}^\top \in \mathbb{R}^{B \times B}$. To prevent self-matches from dominating the probability distribution after softmax when generating soft targets, we remove the diagonal: $\bar{S}_{p,p} = S_{p,p} - \text{diag}(S_{p,p})$. A similar strategy has been adopted in prior work (Gao et al., 2023) for soft target construction and proven effective. *Soft targets* are then defined as

$$\tilde{y}_{ij} = \frac{\exp(\bar{S}_{p,p}[i, j] / \tau_s)}{\sum_{k \neq i} \exp(\bar{S}_{p,p}[i, k] / \tau_s)}, \quad j \neq i, \quad (4)$$

with temperature $\tau_s > 0$. Intuitively, \tilde{y}_{ij} is the probability that pose v_j is a semantically relevant neighbor of v_i in the fixed pose relational graph. Using the same EMG–pose similarities q_{ij} defined earlier for InfoNCE, CASCLe minimizes a *Soft contrastive objective* defined as the cross-entropy between soft targets \tilde{y}_{ij} and q_{ij} , $i \neq j$:

$$\mathcal{L}_{\text{CASCLe}} = -\frac{1}{B} \sum_{i=1}^B \sum_{j=1}^B \tilde{y}_{ij} \log q_{ij}. \quad (5)$$

This objective can be interpreted as predicting the degree of similarity between EMG–pose pairs, where this degree is measured according to the structural organization of the pose latent space. The total training objective of EMBridge combines instance-level and structural community-level supervision:

$$\mathcal{L} = \mathcal{L}_{\text{InfoNCE}} + \alpha \mathcal{L}_{\text{CASCLe}} + \lambda \mathcal{L}_{\text{MPRL}},$$

with weights $\lambda, \alpha > 0$. InfoNCE enforces instance alignment, while CASCLe aligns relational structure of the latent space between two modalities. In this way, the EMG encoder is guided to align not only with its exact pair but also with poses that share similar semantics, providing more robust and informative supervisory signals.

3 EXPERIMENTS AND RESULTS

3.1 EVALUATION PROTOCOLS.

We employ two evaluation protocols to examine the learned representation quality. **Linear probing** (LP): with labeled EMG data $\{(x_i, y_i)\}$, we freeze \mathcal{E}_x and train a randomly-initialized linear

270
271 Table 1: Dataset splits with gesture and user counts. Four unseen gestures evaluated out of six total.
272
273
274
275

Split (totals)	Subset	Gesture Counts		User Counts	
		In-dist.	Unseen	In-dist.	Unseen
\mathcal{D}_{tr} (23 gestures / 158 users)	$\mathcal{D}_{\text{probe-tr}}^{\text{in}}$	4	0	158	0
\mathcal{D}_{val} (29 gestures / 15 users)	$\mathcal{D}_{\text{tune}}$ $\mathcal{D}_{\text{unseen}}$ $\mathcal{D}_{\text{probe-tr}}^{\text{unseen}}$	4 0	4 4	0 0	3 12
\mathcal{D}_{test} (29 gestures / 158 users)	$\mathcal{D}_{\text{eval}}$	4	4	0	20

276
277
278 classifier \mathcal{C} on top of its embeddings, reporting accuracy on a held-out split. **Zero-shot classification** (ZS) is performed as k-nearest-neighbor voting in the embedding space, following standard practice in representation learning (Marks et al., 2024; Radford et al., 2021). For each EMG sample, we retrieve its top- k nearest poses in the embedding space, then vote the corresponding gesture labels to determine the predicted gesture. Given a test EMG sample x_j , let $\mathcal{R}_j = \text{TopK}_{p \in \mathcal{P}_{\text{test}}}(\mathcal{E}_x(x_j)^\top \mathcal{E}_p^*(p))$ be the set of k pose samples with highest cosine similarity to x_j . We then predict $\hat{y}_j = \text{mode}\{y(p) \mid p \in \mathcal{R}_j\}$, where $y(p)$ is the gesture class of pose p .
280
281
282
283
284
285

286
287 3.2 DATASETS
288

289 **emg2pose dataset.** We use *emg2pose* (Salter et al., 2024), a large-scale open-source EMG dataset
290 containing 370 hours of sEMG and synchronized hand pose data across 193 consenting users, 29
291 different behavioral groups that include a diverse range of discrete and continuous hand motions
292 such as making a fist or counting to five. The hand pose labels are generated using a high-resolution
293 motion capture system. The full dataset contains over 80 million pose labels and is of similar scale
294 to the largest computer vision equivalents. Each user completed four recording sessions per gesture
295 category, each with a different EMG-band placement. Each session lasted 45–120 s, during which
296 users repeatedly performed a mix of 3–5 similar gestures or unconstrained freeform movements. We
297 use non-overlapping 2-second windows as input sequences. EMG is instance-normalized, band-pass
298 filtered (2–250 Hz), and notch-filtered at 60 Hz. For more details, please refer to Salter et al. (2024).
299

300 **Data Split for emg2pose.** We evaluate on two disjoint gesture sets drawn from the public *emg2pose*
301 corpus. First, we select four representative single-hand motions covering various finger movements
302 as our **in-distribution gestures**. Second, from the six held-out classes that are not seen during training,
303 we exclude the two-handed gesture and the highly variable “finger freeform” class, yielding four
304 **unseen gestures**. Details of gesture classes are in Appendix. For data splits, we follow the public
305 train \mathcal{D}_{tr} , val \mathcal{D}_{val} , test \mathcal{D}_{test} splits and define our data splits for downstream gesture classification
306 tasks as shown in Table 1. The model is pre-trained on the full \mathcal{D}_{tr} . A linear head is trained on
307 $\mathcal{D}_{\text{probe-tr}}^{\text{in}}$, and report final accuracy on the evaluation set $\mathcal{D}_{\text{eval}}^{\text{in}}$. For linear probing on unseen gestures
308 (which appear only in the original val and test splits), we train on $\mathcal{D}_{\text{probe-tr}}^{\text{unseen}}$, and report accuracy on
309 $\mathcal{D}_{\text{eval}}^{\text{unseen}}$. Zero-shot classification is evaluated only on $\mathcal{D}_{\text{eval}}$. All users in $\mathcal{D}_{\text{eval}}$ are unseen, so both
310 the LP and ZS results also assess user-level generalization. A held-out dataset $\mathcal{D}_{\text{tune}}$, strictly disjoint
311 from all other sets, is reserved for hyper-parameter tuning.
312

313 **NinaPro dataset:** We utilized two *NinaPro* EMG datasets for a more comprehensive evaluation of
314 EMBridge. Specifically, Ninapro DB2 (Atzori et al., 2014) is used for pre-training, which includes
315 paired EMG-pose data from 40 subjects. It contains 49 hand gestures (including basic finger flexions,
316 functional grasps, and combined movements) performed by 40 healthy subjects. EMG signals
317 are recorded from 12 electrodes placed on the forearm at a sampling rate of 2 kHz, alongside hand
318 kinematics data captured by a data glove. For downstream gesture classification, we use NinaPro
319 DB7 (Krasoulis et al., 2017), which contains data from 20 non-amputated subjects collected with
320 the same EMG device and gesture set as DB2 (more details on NinaPro Website¹). **Data split.** The
321 entire DB2 dataset was used for pre-training, except Gestures 1, 5, 10, and 15 from exercise B,
322 which were excluded to serve as **unseen gestures** in DB7. Gestures 1, 5, 10, and 10 from exercise
323 C were used as **in-distribution gestures**. Within each gesture, sessions were randomly divided into
324 probe-training and evaluation sets, and zero-shot evaluation was conducted only on the latter.
325

¹<https://nинapro.hevs.ch/>

324 3.3 GESTURE CLASSIFICATION RESULTS
325

326 **Comparing Schemes.** We evaluate EMBridge against various baselines. Unimodal models trained
327 solely on EMG include: a supervised encoder–decoder Transformer (**PoseT**) regressing poses
328 from EMG; the supervised regression models from the *emg2pose* benchmark (Salter et al., 2024)
329 (**emg2pose**, **Vemg2pose**, **NeuroPose**); and a self-supervised MAE model trained only on EMG
330 (**EMG-MAE**). We also compare to multi-modal models: a CLIP-style Contrastive Pose–EMG Pre-
331 training framework (**CPEP**), which applies $\mathcal{L}_{\text{InfoNCE}}$ directly to [CLS] tokens from EMG and pose
332 encoders via a projection layer; and a plain **Q-Former** variant trained only with $\mathcal{L}_{\text{InfoNCE}}$. Unlike
333 **Q-Former**, **CPEP** does not introduce a transformer but uses a projection layer. We further evaluate
334 label-smoothed variants of both models. Label smoothing has been shown to improve contrastive
335 learning by mitigating overconfidence and handling noisy similarities (Wickstrøm et al., 2022; Li
336 et al., 2022). We introduce **CPEP-LS** and **Q-Former-LS**, where InfoNCE targets are softened with
337 a smoothing factor of 0.1. For a fair comparison under linear probing, each baseline’s encoder is
338 frozen and a softmax linear head is trained on top. As an additional reference, we report an **upper
339 bound** from linear probing the pre-trained Pose-MAE. Since the pose encoder is the fixed alignment
340 anchor, this represents the best achievable performance if EMG features were perfectly aligned. For
341 LP, we use publicly available *emg2pose* checkpoints with the same data splits.

342 We evaluate EMG representation quality on both **in-dist.** and **unseen** gestures using two protocols:
343 zero-shot classification (ZS) and linear probing (LP). Supervised baselines do not support zero-shot
344 (K-nearest neighbor) classification in the embedding space. We report balanced accuracy on both
345 *emg2pose* and *NinaPro* dataset to account for class imbalance across gesture classes. As shown in
346 Table 2, EMBridge consistently outperforms all baselines, with the largest gains in zero-shot classi-
347 fication, where it even surpasses the LP performance of all unimodal models. The most significant
348 improvements appear on unseen gestures for *emg2pose* and ZS on in-dist. gestures for *NinaPro*,
349 demonstrating the stronger generalization capacity of EMBridge and its practical value for wear-
350 able gesture recognition. We note that **CPEP** achieves higher LP performance on unseen gestures
351 than EMBridge for both datasets. This is likely due to our use of query averaging in EMBridge
352 instead of selecting the query with maximum similarity to the paired pose, which may be subopti-
353 mal. Maximum-similarity selection is avoided here during LP to prevent potential data leakage. We
354 also evaluate EMBridge in the few-shot setting with LP on *emg2pose*. Even with only 50% of the
355 probe-training data, EMBridge outperforms all unimodal baselines.²

356 Table 2: Comparison of gesture classification results across unimodal and multi-modal models.
357 Results are reported on the *emg2pose* dataset and the *NinaPro* dataset.

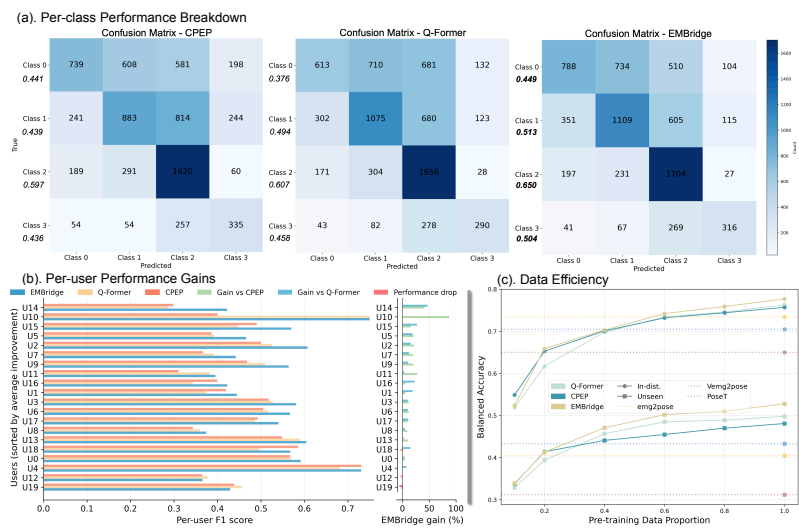
358 Unimodal Models	359 <i>emg2pose</i>				360 <i>NinaPro</i>			
	361 In-dist. LP		362 Unseen LP		363 In-dist. LP		364 Unseen LP	
365 Upper-bound	0.851		0.649		0.769		0.632	
366 EMG-MAE	0.347		0.334		0.283		0.256	
367 NeuroPose (Salter et al., 2024)	0.692		0.248		/		/	
368 emg2pose (Salter et al., 2024)	0.734		0.405		/		/	
369 Vemg2pose (Salter et al., 2024)	0.650		0.312		/		/	
370 PoseT	0.705		0.433		0.694		0.425	
371 Multi-modal Models	372 In-dist.		373 Unseen		374 In-dist.		375 Unseen	
	376 LP	ZS	377 LP	ZS	378 LP	ZS	379 LP	ZS
380 CPEP	0.782		0.757		0.536		0.481	
381 CPEP-LS	0.780		0.759		0.538		0.487	
382 Q-Former	0.782		0.763		0.493		0.498	
383 Q-Former-LS	0.777		0.760		0.495		0.498	
384 EMBridge	0.785		0.777		0.505		0.528	
385							0.703	
386							0.692	
387							0.492	
388							0.447	

389 **Per-Gesture Classification Performance Breakdown.** We conduct a detailed analysis on the
390 *emg2pose* dataset by computing per-gesture F1 scores from zero-shot classification on unseen ges-
391 tures to assess performance gains achieved by EMBridge over other cross-modal frameworks (CPEP
392

393 ²More details are provided in the Appendix.

378 and Q-Former). Reporting F1 scores provides a more comprehensive and balanced view of per-class
 379 performance. Confusion matrices in Figure 3(a) offer a clearer illustration of improvements. Com-
 380 pared to CPEP and Q-Former, **EMBridge achieves consistently higher F1 scores across all ges-
 381 ture classes**, with particularly notable gains on *Class 1* (0.513 vs. 0.439/0.494) and *Class 3* (0.504
 382 vs. 0.436/0.458). *Class 3* is the gesture of counting up and down then finger wiggling, which is very
 383 challenging for vision-based gesture classification due to visual occlusion (Salter et al., 2024). The
 384 improvements underscore EMBridge’s stronger discriminative capability on difficult and frequently
 385 confused gestures, demonstrating its practical value in real-world cases where occlusion is common.

386 **Per-User Performance Gains Breakdown.** Similarly, on unseen gestures, we compute the zero-
 387 shot classification performance (F1 score) within each user, where all 20 users are held out from
 388 training. Figure 3(b) illustrates the per-user performance gains of EMBridge compared to CPEP and
 389 Q-Former. For per-user analysis, EMBridge achieves an overall improvement of 14.2% over CPEP
 390 (0.522 vs. 0.457) and 10.2% over Q-Former (0.522 vs. 0.473). The average relative per-user im-
 391 provement is 16.0% compared to CPEP and 11.6% compared to Q-Former, which demonstrates that
 392 EMBridge yields consistent improvements across unseen users, even under inter-subject variability.



411 Figure 3: (a) Confusion matrices from ZS on unseen gestures, with per-class *F1 scores* shown beside
 412 row labels. (b) Per-user ZS performance on unseen gestures. (c) Data efficiency analysis via ZS on
 413 in-dist. and unseen gestures. Dotted lines indicate LP performance of unimodal baselines.

4 ABLATION STUDY

417 **Individual Contribution of Components in EMBridge.** We analyze three ablated variants of EM-
 418 Bridge, each removing a component (Q-Former, MPRL, or CASCLe) to assess its individual impact.
 419 Removing Q-Former reduces the model to CPEP + CASCLe, since without the Q-Former architec-
 420 ture and learnable queries, the masked pose reconstruction task cannot be performed. As shown in
 421 Table 3, removing any component leads to a drop in zero-shot performance. Interestingly, remov-
 422 ing Q-Former yields slightly better linear probing results, consistent with prior CPEP findings, and
 423 demonstrates the versatility of CASCLe that it can be effectively integrated into the CPEP archi-
 424 tecture to improve performance. Removing MPRL or CASCLe reduces generalization to unseen
 425 gestures, underscoring their importance in cross-modal alignment and representation learning.

426 **Soft Contrastive Objectives.** We further compare CASCLe with alternative soft contrastive learn-
 427 ing objectives. **Label Smoothing**, explored in Fini et al. (2023), applies soft targets in CLIP and
 428 has shown consistent gains. We also adapt SoftCLIP (Gao et al., 2023) to our EMG–pose setup
 429 by deriving soft targets from **instance-level** pairwise similarities between pose samples, providing
 430 a fair baseline against CASCLe, which models community-level structural similarity. We replace
 431 $\mathcal{L}_{\text{InfoNCE}} + \alpha \mathcal{L}_{\text{CASCLe}}$ with label smoothing and the adapted SoftCLIP objective, respectively, while
 keeping the rest of EMBridge unchanged. Further discussion of soft contrastive learning is provided

432

433

Table 3: Ablation of EMBridge: individual component impact and soft contrastive objectives.

434

435

436

437

438

439

440

441

442

443

444

445

446

in Section 5. In Table 3, CASCLe outperforms both alternatives in ZS, which highlights the advantage of modeling community structure over simple soft labels or instance-level similarities.

447

Data Efficiency. We investigate how the scale of paired pre-training data influences downstream performance. Since collecting paired EMG-pose data is costly and time-consuming, it is essential to evaluate the data efficiency of EMBridge. We uniformly downsample sessions within each gesture class to simulate limited pre-training data. We vary the proportion of paired pre-training data from 0.2 to 1.0 (full dataset) and report ZS performance on both in-dist. and unseen gestures in Figure 3(c). Remarkably, even when trained with only 40% of the paired data, EMBridge’s zero-shot classification still surpasses the LP performance of unimodal baselines trained on the full dataset.

448

449

450

451

452

453

454

455

456

457

458

459

460

461

462

463

464

465

466

467

468

469

470

471

472

473

474

475

476

477

478

479

480

481

482

483

484

485

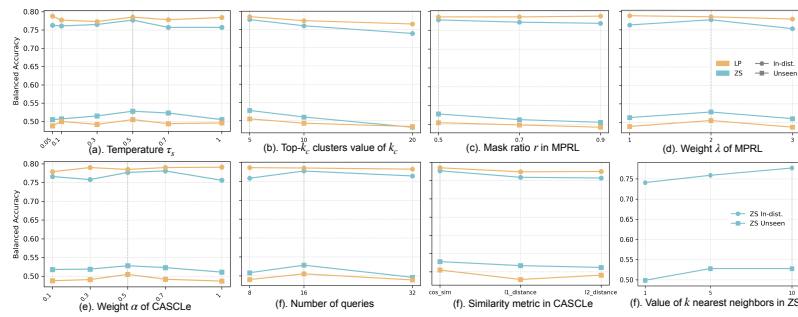


Figure 4: Sensitivity to hyper-parameters. Dashed lines indicate the values used in the best setup.

486 5 DISCUSSION AND CONCLUSION
487488
489 **Related Work on Soft Contrastive Learning.** Traditional contrastive learning methods (van den
490 Oord et al., 2019; Chen et al., 2020; Radford et al., 2021) use one-hot targets, where only the exact
491 matching pair is treated as positive and all others as negatives. However, when multiple positives or
492 highly similar instances exist, this introduces false negatives. Recent work addresses this by incor-
493 porating soft targets. Fini et al. (2023) employs label smoothing to generate soft targets. SoftCLIP
494 (Gao et al., 2023) derives them from intra-modal similarity using fine-grained image features, while
495 X-CLR (Sobal et al., 2024) builds a sample similarity graph and replaces binary labels with simi-
496 larity scores. SoftCLT (Lee et al., 2024b) softens targets based on temporal proximity, and Huang
497 et al. (2024) aligns cross-modal and uni-modal representations using teacher-derived similarity sig-
498 nals. **CASCLe** differs by constructing soft targets from **community-level** structural similarities in
499 the embedding space, rather than relying solely on instance-level relations.500 The motivation of asymmetric setup is to use pose representations as fixed anchors to guide the
501 learning of EMG representations. Training both encoders simultaneously could lead to suboptimal
502 representations, as the pose representations are altered to be closer to the noisier EMG represen-
503 tations. Additionally, this asymmetric setup enhances extendability. Future work can pre-train the
504 pose encoder on large-scale and unpaired pose data using MAE. This allows us to effectively learn
505 EMG representations by aligning with frozen pose embeddings, even when paired data is limited.
506 Leveraging abundant unpaired data reduces reliance on paired samples and improves data efficiency.507 By leveraging pose as a rich supervisory signal, EMBridge learns pose-informed EMG embed-
508 dings that capture structural and semantic relationships and are discriminative in the latent space.
509 Across in-distribution and unseen gesture classification tasks, EMBridge demonstrated strong per-
510 formance gains, particularly in zero-shot setting. Overall, EMBridge provides an effective approach
511 to zero-shot gesture classification on wearable EMG signals, and can serve as a foundation for future
512 exploration of cross-modal representation learning on EMG and other bio-signals.513
514 6 LIMITATIONS AND FUTURE WORK
515516
517 While EMBridge significantly enhances zero-shot gesture classification on wearable EMG signals,
518 we acknowledge limitations and room for future explorations. Our framework currently relies on
519 paired EMG-pose data for cross-modal alignment. Although *emg2pose* and *NinaPro* are large-scale
520 datasets, high-quality paired datasets remain scarce in the broader bio-signal community. Training
521 on a single dataset could potentially limit the pose encoder’s capacity. A promising direction for fu-
522 ture work is to leverage large-scale, publicly available unpaired pose data for unimodal pre-training.
523 This would yield more robust pose representations, providing stronger supervision for EMG repre-
524 sentation learning while significantly reducing the reliance on paired samples. EMBridge can further
525 demonstrate its effectiveness in cross-modal learning with limited paired data. Furthermore, the pro-
526 posed framework can potentially be extended to other modalities such as RGB-EMG or Video-EMG
527 in future work, which can be done by incorporating a pre-trained vision encoder.528 Another interesting direction for future work is to explore probabilistic modeling when constructing
529 pose communities. Specifically, a Gaussian Mixture Model could be used to assign each pose em-
530 bedding a soft probability distribution over multiple clusters or communities. Structural similarity
531 between poses could then be computed based on the similarity between these membership distri-
532 butions (e.g., using KL divergence), enabling a smoother and more continuous modeling of pose
533 neighborhood structure. This may better capture complex pose dynamics.534
535 7 REPRODUCIBILITY STATEMENT
536537
538 All datasets used in this work are publicly available. Details of the model architecture, training
539 objectives, and implementation details are provided in Section 2 and Appendix A.6, including all
key hyper-parameters and model configurations to ensure reproducibility.

540 REFERENCES
541

542 Manfredo Atzori, Arjan Gijsberts, Claudio Castellini, Barbara Caputo, Anne-Gabrielle Mittaz
543 Hager, Simone Elsig, Giorgio Giatsidis, Franco Bassetto, and Henning Müller. Electromyog-
544 raphy data for non-invasive naturally-controlled robotic hand prostheses. *Scientific data*, 1(1):
545 1–13, 2014.

546 Manfredo Atzori, Arjan Gijsberts, Claudio Castellini, Barbara Caputo, Anne-Gabrielle Hager,
547 Stephan Elsig, Giorgio Giatsidis, Franco Bassetto, and Henning Müller. Deep learning with
548 convolutional neural networks applied to electromyography data: A resource for the classification
549 of movements for prosthetic hands. *Frontiers in Neurorobotics*, 10:9, 2016.

550 Antonino Casile, Giulia Fregna, Vittorio Boarini, Chiara Paoluzzi, Fabio Manfredini, Nicola Lam-
551 bertini, Andrea Baroni, and Sofia Straudi. Quantitative comparison of hand kinematics measured
552 with a markerless commercial head-mounted display and a marker-based motion capture system
553 in stroke survivors. *Sensors*, 23(18):7906, 2023.

554 Ting Chen, Simon Kornblith, Mohammad Norouzi, and Geoffrey Hinton. A simple framework
555 for contrastive learning of visual representations, 2020. URL <https://arxiv.org/abs/2002.05709>.

556 Xiachong Feng, Xiaocheng Feng, Bing Qin, and Ting Liu. Aligning semantic in brain and lan-
557 guage: A curriculum contrastive method for electroencephalography-to-text generation. *IEEE*
558 *Transactions on Neural Systems and Rehabilitation Engineering*, 31:3874–3883, 2023. doi:
559 10.1109/TNSRE.2023.3314642.

560 Enrico Fini, Pietro Astolfi, Adriana Romero-Soriano, Jakob Verbeek, and Michal Drozdzal. Im-
561 proved baselines for vision-language pre-training, 2023. URL <https://arxiv.org/abs/2305.08675>.

562 Yuting Gao, Jinfeng Liu, Zihan Xu, Tong Wu Enwei Zhang, Wei Liu, Jie Yang, Ke Li, and Xing Sun.
563 Softclip: Softer cross-modal alignment makes clip stronger, 2023. URL <https://arxiv.org/abs/2303.17561>.

564 Yuxin Guo, Shuailei Ma, Shijie Ma, Xiaoyi Bao, Chen-Wei Xie, Kecheng Zheng, Tingyu Weng,
565 Siyang Sun, Yun Zheng, and Wei Zou. Aligned better, listen better for audio-visual large language
566 models, 2025. URL <https://arxiv.org/abs/2504.02061>.

567 Sumanth Gurram, Andy Fang, David Chan, and John Canny. Lava: Language audio vision align-
568 ment for contrastive video pre-training, 2022. URL <https://arxiv.org/abs/2207.08024>.

569 Kaiming He, Xinlei Chen, Saining Xie, Yanghao Li, Piotr Dollár, and Ross Girshick. Masked
570 autoencoders are scalable vision learners, 2021. URL <https://arxiv.org/abs/2111.06377>.

571 Hailang Huang, Zhijie Nie, Ziqiao Wang, and Ziyu Shang. Cross-modal and uni-modal soft-label
572 alignment for image-text retrieval. *Proceedings of the AAAI Conference on Artificial Intelligence*,
573 38(16):18298–18306, March 2024. ISSN 2159-5399. doi: 10.1609/aaai.v38i16.29789. URL
574 <http://dx.doi.org/10.1609/aaai.v38i16.29789>.

575 Néstor J Jarque-Bou, Joaquin L Sancho-Bru, and Margarita Vergara. A systematic review of emg
576 applications for the characterization of forearm and hand muscle activity during activities of daily
577 living: Results, challenges, and open issues. *Sensors*, 21(9):3035, 2021.

578 Prannay Khosla, Piotr Teterwak, Chen Wang, Aaron Sarna, Yonglong Tian, Phillip Isola, Aaron
579 Maschinot, Ce Liu, and Dilip Krishnan. Supervised contrastive learning, 2021. URL <https://arxiv.org/abs/2004.11362>.

580 Agamemnon Krasoulis, Iris Kyranou, Mustapha Suphi Erden, Kianoush Nazarpour, and Sethu Vi-
581 jayakumar. Improved prosthetic hand control with concurrent use of myoelectric and inertial
582 measurements. *Journal of neuroengineering and rehabilitation*, 14(1):71, 2017.

594 Gierad Laput and Chris Harrison. Sensing fine-grained hand activity with smartwatches. In *Proceedings of the 2019 CHI Conference on Human Factors in Computing Systems*, CHI '19, pp. 1–13,
 595 New York, NY, USA, 2019. Association for Computing Machinery. ISBN 9781450359702. doi:
 596 10.1145/3290605.3300568. URL <https://doi.org/10.1145/3290605.3300568>.
 597

598 Donghee Lee, Dayoung You, Gyoungryul Cho, Hoirim Lee, Eunsoo Shin, Taehwan Choi, Sung-
 599 han Kim, Sangmin Lee, and Woochul Nam. Emg-based hand gesture classifier robust to daily
 600 variation: Recursive domain adversarial neural network with data synthesis. *Biomedical Signal
 601 Processing and Control*, 88:105600, 2024a.
 602

603 Seunghan Lee, Taeyoung Park, and Kibok Lee. Soft contrastive learning for time series, 2024b.
 604 URL <https://arxiv.org/abs/2312.16424>.
 605

606 Junnan Li, Dongxu Li, Caiming Xiong, and Steven Hoi. Blip: Bootstrapping language-image
 607 pre-training for unified vision-language understanding and generation, 2022. URL <https://arxiv.org/abs/2201.12086>.
 608

609 Junnan Li, Dongxu Li, Silvio Savarese, and Steven Hoi. BLIP-2: bootstrapping language-image
 610 pre-training with frozen image encoders and large language models. In *ICML*, 2023.
 611

612 Aristidis Likas, Nikos Vlassis, and Jakob J Verbeek. The global k-means clustering algorithm.
 613 *Pattern recognition*, 36(2):451–461, 2003.
 614

615 Yilin Liu, Shijia Zhang, and Mahanth Gowda. Neuropose: 3d hand pose tracking using emg
 616 wearables. In *Proceedings of the Web Conference 2021*, WWW '21, pp. 1471–1482, New
 617 York, NY, USA, 2021. Association for Computing Machinery. ISBN 9781450383127. doi:
 618 10.1145/3442381.3449890. URL <https://doi.org/10.1145/3442381.3449890>.
 619

620 Ilya Loshchilov and Frank Hutter. Sgdr: Stochastic gradient descent with warm restarts, 2017. URL
 621 <https://arxiv.org/abs/1608.03983>.
 622

623 Ilya Loshchilov and Frank Hutter. Decoupled weight decay regularization, 2019. URL <https://arxiv.org/abs/1711.05101>.
 624

625 S Marcos-Antón et al. semg-controlled forearm bracelet and serious game-based rehabilitation.
Journal of NeuroEngineering and Rehabilitation, 2023. URL <https://jneuroengrehab.biomedcentral.com/articles/10.1186/s12984-023-01233-5>.
 626

627 Markus Marks, Manuel Knott, Neehar Kondapaneni, Elijah Cole, Thijs Defraeye, Fernando Perez-
 628 Cruz, and Pietro Perona. A closer look at benchmarking self-supervised pre-training with image
 629 classification, 2024. URL <https://arxiv.org/abs/2407.12210>.
 630

631 Ali Moin, Andy Zhou, Abbas Rahimi, Alisha Menon, Simone Benatti, George Alexandrov, Senam
 632 Tamakloe, Jonathan Ting, Natasha Yamamoto, Yasser Khan, et al. A wearable biosensing system
 633 with in-sensor adaptive machine learning for hand gesture recognition. *Nature Electronics*, 4(1):
 54–63, 2021.
 634

635 Mansooreh Montazerin, Elahe Rahimian, Farnoosh Naderkhani, S Farokh Atashzar, Svetlana
 636 Yanushkevich, and Arash Mohammadi. Transformer-based hand gesture recognition from in-
 637 instantaneous to fused neural decomposition of high-density emg signals. *Scientific reports*, 13(1):
 638 11000, 2023.
 639

640 Seungwhan Moon, Andrea Madotto, Zhaojiang Lin, Alireza Dirafzoon, Aparajita Saraf, Amy Bear-
 641 man, and Babak Damavandi. Imu2clip: Multimodal contrastive learning for imu motion sensors
 642 from egocentric videos and text, 2022. URL <https://arxiv.org/abs/2210.14395>.
 643

644 Georgios Pavlakos, Dandan Shan, Ilija Radosavovic, Angjoo Kanazawa, David Fouhey, and Jitendra
 645 Malik. Reconstructing hands in 3d with transformers, 2023. URL <https://arxiv.org/abs/2312.05251>.
 646

647 Joao Pereira, Dimitrios Chalatsis, Balint Hodossy, and Dario Farina. Tackling electrode shift in
 648 gesture recognition with hd-emg electrode subsets, 2024. URL <https://arxiv.org/abs/2401.02773>.
 649

648 Kyung Rok Pyun, Kangkyu Kwon, Myung Jin Yoo, Kyun Kyu Kim, Dohyeon Gong, Woon-Hong
 649 Yeo, Seungyong Han, and Seung Hwan Ko. Machine-learned wearable sensors for real-time
 650 hand-motion recognition: toward practical applications. *National science review*, 11(2):nwad298,
 651 2024.

652

653 Jing Qi, Li Ma, Zhenchao Cui, and Yushu Yu. Computer vision-based hand gesture recognition for
 654 human-robot interaction: a review. *Complex & Intelligent Systems*, 10(1):1581–1606, 2024.

655

656 Alec Radford, Jong Wook Kim, Chris Hallacy, Aditya Ramesh, Gabriel Goh, Sandhini Agar-
 657 wal, Girish Sastry, Amanda Askell, Pamela Mishkin, Jack Clark, Gretchen Krueger, and Ilya
 658 Sutskever. Learning transferable visual models from natural language supervision, 2021. URL
 659 <https://arxiv.org/abs/2103.00020>.

660

661 Sasha Salter, Richard Warren, Collin Schlager, Adrian Spurr, Shangchen Han, Rohin Bhasin, Yujun
 662 Cai, Peter Walkington, Anuoluwapo Bolarinwa, Robert Wang, Nathan Danielson, Josh Merel,
 663 Eftychios Pnevmatikakis, and Jesse Marshall. emg2pose: A large and diverse benchmark for
 664 surface electromyographic hand pose estimation, 2024. URL <https://arxiv.org/abs/2412.02725>.

665

666 Vlad Sobal, Mark Ibrahim, Randall Balestrieri, Vivien Cabannes, Diane Bouchacourt, Pietro As-
 667 tolfi, Kyunghyun Cho, and Yann LeCun. X-sample contrastive loss: Improving contrastive learn-
 668 ing with sample similarity graphs, 2024. URL <https://arxiv.org/abs/2407.18134>.

669

670 Simon Tam, Shriram Tallam Puranam Raghu, Étienne Buteau, Erik Scheme, Mounir Boukadoum,
 671 Alexandre Campeau-Lecours, and Benoit Gosselin. Towards robust and interpretable emg-based
 672 hand gesture recognition using deep metric meta learning, 2024. URL <https://arxiv.org/abs/2404.15360>.

673

674 Rayane Tchantchane, Hao Zhou, Shen Zhang, and Gursel Alici. A review of hand gesture recog-
 675 nition systems based on noninvasive wearable sensors. *Advanced intelligent systems*, 5(10):
 676 2300207, 2023.

677

678 Aaron van den Oord, Yazhe Li, and Oriol Vinyals. Representation learning with contrastive predic-
 679 tive coding, 2019. URL <https://arxiv.org/abs/1807.03748>.

680

681 Laurens Van der Maaten and Geoffrey Hinton. Visualizing data using t-sne. *Journal of machine
 682 learning research*, 9(11), 2008.

683

684 Ashish Vaswani, Noam Shazeer, Niki Parmar, Jakob Uszkoreit, Llion Jones, Aidan N. Gomez,
 685 Lukasz Kaiser, and Illia Polosukhin. Attention is all you need, 2023. URL <https://arxiv.org/abs/1706.03762>.

686

687 Huihui Wang, Bo Ru, Xin Miao, Qin Gao, Masood Habib, Long Liu, and Sen Qiu. Mems devices-
 688 based hand gesture recognition via wearable computing. *Micromachines*, 14(5):947, 2023.

689

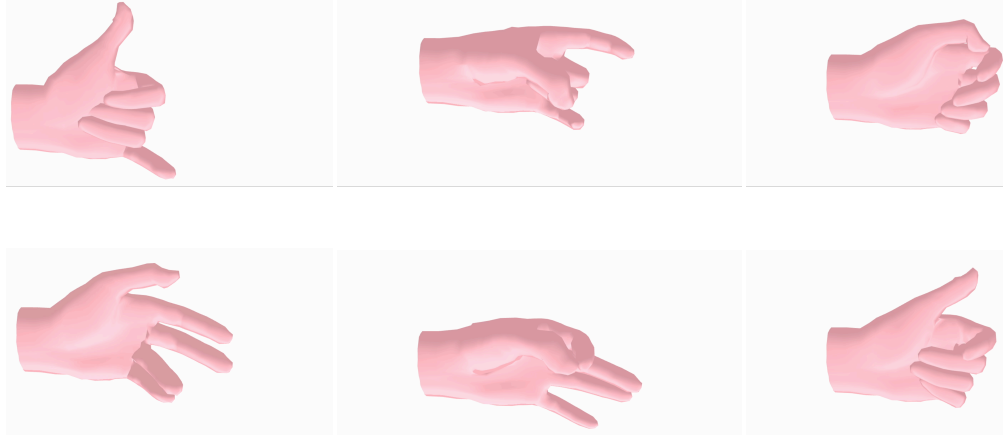
690 Kristoffer Wickstrøm, Michael Kampffmeyer, Karl Øyvind Mikalsen, and Robert Jenssen. Mixing
 691 up contrastive learning: Self-supervised representation learning for time series. *Pattern Recog-
 692 nition Letters*, 155:54–61, March 2022. ISSN 0167-8655. doi: 10.1016/j.patrec.2022.02.007. URL
 693 <http://dx.doi.org/10.1016/j.patrec.2022.02.007>.

694

695 Shaoan Xie, Lingjing Kong, Yujia Zheng, Yu Yao, Zeyu Tang, Eric P. Xing, Guangyi Chen, and
 696 Kun Zhang. Smartclip: Modular vision-language alignment with identification guarantees, 2025.
 697 URL <https://arxiv.org/abs/2507.22264>.

698

699 Guangjie Yu, Ziting Deng, Zhenchen Bao, Yue Zhang, and Bingwei He. Gesture classification
 700 in electromyography signals for real-time prosthetic hand control using a convolutional neural
 701 network-enhanced channel attention model. *Bioengineering*, 10(11):1324, 2023.

702 **A APPENDIX**
703704 **A.1 THE USE OF LARGE LANGUAGE MODELS (LLMs)**
705706 We used LLMs to assist with language polishing, including grammar checking and word choice
707 refinement. All research ideas, experiment design, analyses, and essential contributions were con-
708 ducted by the authors.710 **A.2 DETAILS OF EMG2POSE DATASET**
711712 **A.2.1 DATA COLLECTION PROTOCOL**713 Data collection was divided into four distinct sessions, involving multiple device don-doff cycles
714 (avg. 3.9) to account for sensor placement shifts. In each session, participants performed two repeti-
715 tions of prompted stages (gesture categories), with each stage lasting 45 to 60 seconds. Annotations
716 are available at this recording level, which we utilized as the gesture class labels. Each stage con-
717 tains either a mix of discrete gestures or freeform unprompted movements. To ensure a broad range
718 of postures, participants were explicitly instructed to move their hand from right-to-left and up-and-
719 down while performing specific gestures.721 **A.2.2 DETAILS OF GESTURES**722 **In-distribution (4 classes).** 80 sessions per-class. *class 0*: Thumb swipes whole hand; *class 1*:
723 Hand claw, grasp, and flicks. *class 2*: ThumbsUpDown, ThumbRotations; *class 3*: FingerPinches,
724 SingleFinger, PinchesMultiple;725
726 **Unseen (4 classes).** *class 0*: HookEmHorns, OK, and Scissors (80 sessions); *class 1*: Shaka
727 and Vulcan peace (80 sessions); *class 2*: Counting up/down face side away (80 sessions); *class 3*:
728 Counting up/down with finger wiggling and spreading (40 sessions).745 Figure 5: Example visualizations of gestures used in gesture classification tasks.
746747 **A.3 VISUALIZATION OF REPRESENTATIONS.**
748749 We visualize EMG embeddings before and after applying EMBridge using t-SNE (Van der Maaten
750 & Hinton, 2008), and compare them with anchor pose embeddings from the pre-trained Pose-MAE.
751 Points are colored by gesture classes. Before EMBridge, EMG embeddings (pre-trained with MAE),
752 show mixed distributions across classes. After EMBridge, the EMG embeddings become more
753 structured and separable across classes. As we observe in the pose space, some overlap between
754 classes remains, which reflects micro-gestures within 2-second windows that share semantic simi-
755 larity across gesture categories. This highlights both the improved alignment achieved by EMBridge
and the intrinsic difficulty of gesture classification on this dataset.

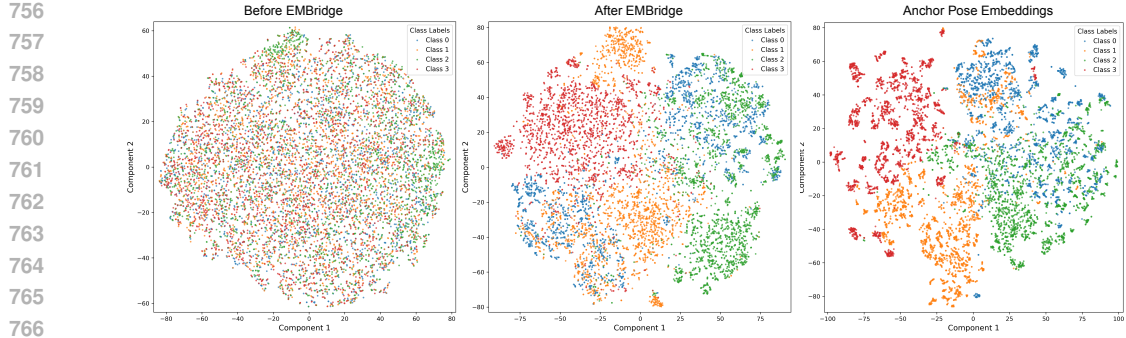


Figure 6: t-SNE visualization of embeddings from in-dist. gestures, colored by gesture class labels.

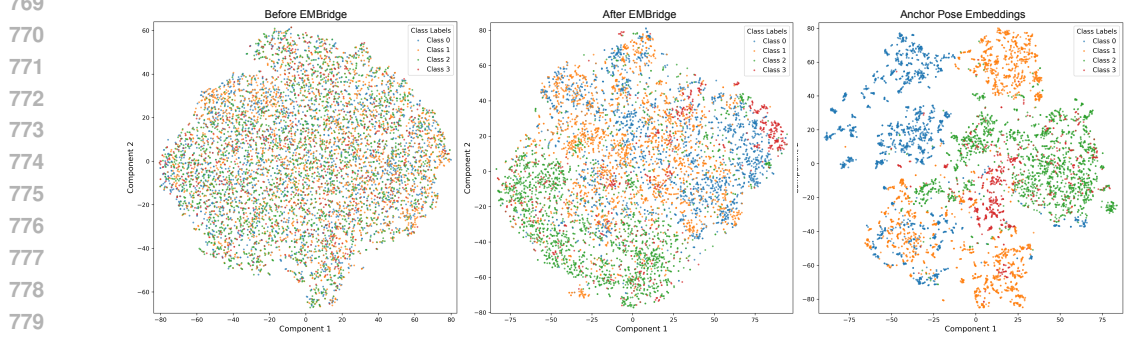


Figure 7: t-SNE visualization of embeddings from unseen gestures, colored by gesture class labels.

A.4 FEW-SHOT EVALUATION OF EMBRIDGE

We evaluate the few-shot performance of EMBridge by gradually increasing the number of training samples within each class (n-shot) during linear probing. For each number of shots, we repeat random sampling five times to obtain a more reliable estimate of performance. We report the average balanced accuracy, with the standard deviation indicated as a shaded region in Figure 8. With only 50% of the probe-training data (40 shots), EMBridge can achieve performance almost comparable to that of the full set on unseen gestures and surpasses all baselines trained on the complete dataset.

A.5 VISUALIZATION OF SOFT TARGETS CONSTRUCTED IN CASCLE

We visualize the soft targets to examine how the temperature τ_s and the number of top- k clusters k_c influence the resulting probability distribution. As shown in Figure 9, a smaller τ_s produces a sharper distribution, where probability mass is concentrated on a few dominant samples. This indicates that the model places high confidence on a small number of nearest pose neighbors, approaching a hard-label regime. In contrast, a larger τ_s leads to a smoother distribution with more evenly distributed weights, reflecting greater uncertainty and incorporating information from a broader set of pose samples. For the number of clusters k_c , larger values expands the set of contributing clusters and potentially diluting the impact of the most similar samples.

A.6 IMPLEMENTATION DETAILS

We use 2 s windows sampled at 2 kHz for both pose and EMG. EMG is instance-normalized, band-pass filtered (2–250 Hz), and notch-filtered at 60 Hz. Following (Salter et al., 2024), we apply channel-rotation augmentation to EMG. Our MAE is a encoder–decoder Transformer model with 4 encoder layers and 2 decoder layers, and the embedding dimension is $d=256$. We optimize with AdamW (Loshchilov & Hutter, 2019) ($\text{lr } 1\text{e-}4$, weight decay $1\text{e-}5$) and cosine annealing with warm restarts (Loshchilov & Hutter, 2017). The masking ratio is 50%. Token length is $S=200$ for pose and $S=50$ for EMG, producing non-overlapping tokens along time. Mask ratio $r = 0.5$. Each

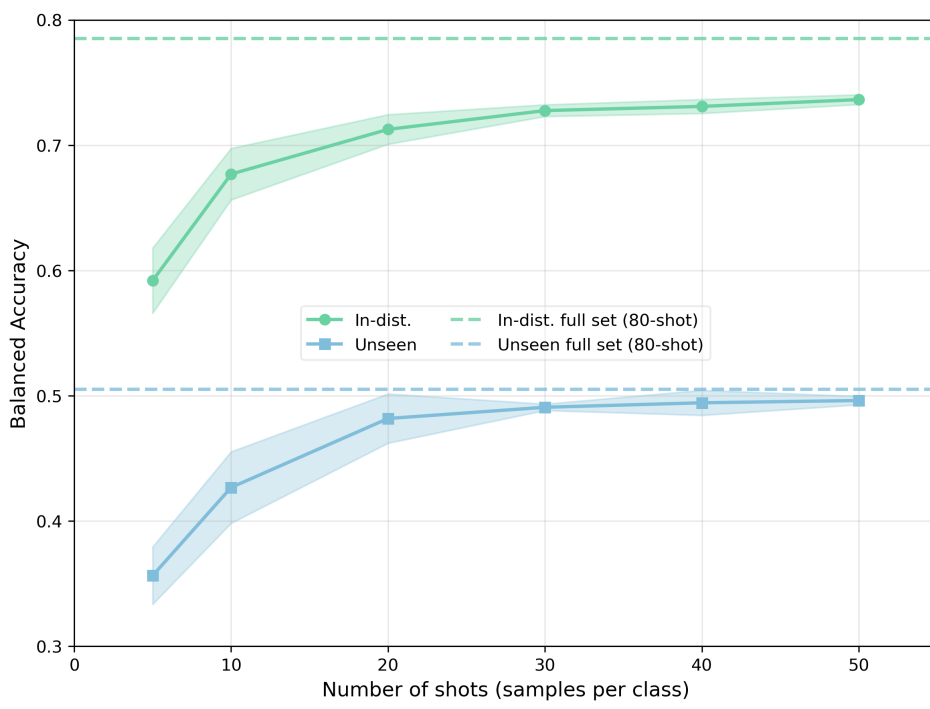


Figure 8: Few-shot evaluation of EMBridge. X-axis is the number of training samples within each class (n-shot) during linear probing. For each number of shots, we repeat random sampling five times to obtain a more reliable estimate of performance. We report the average balanced accuracy, with the standard deviation indicated as a shaded region.

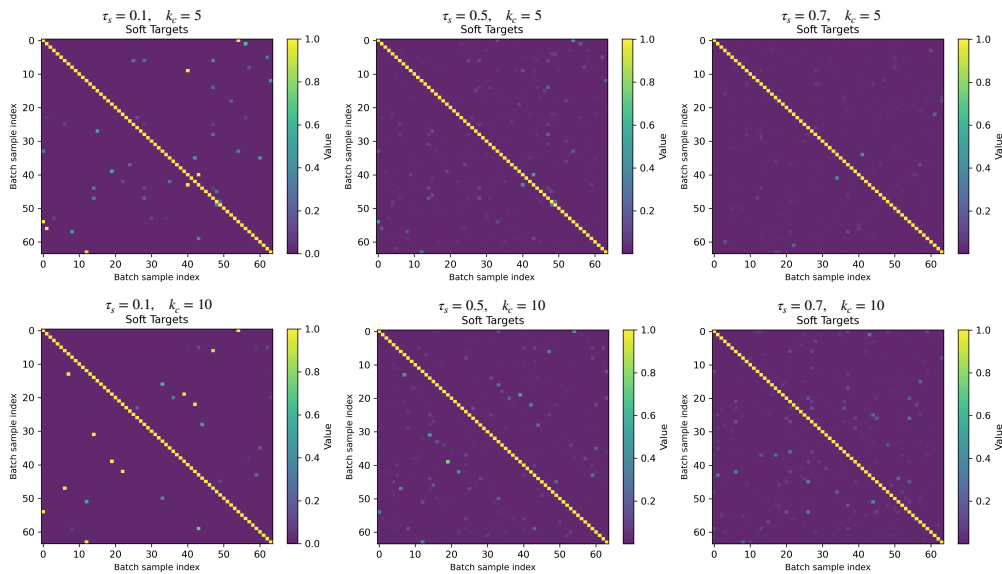


Figure 9: Soft targets from a batch of 64 samples for clearer visualization. We vary the value of temperature τ_s and the number of top-k clusters k_c .

864 MAE is trained for 100 epochs. PoseT is a encoder-decoder transformer model that consists of 4
 865 encoder layers and 2 decoder layers, trained using the same losses adopted in Salter et al. (2024).
 866

867 For CPEP, we attach a 1-layer projection head (hidden size 256) to the EMG encoder and train the
 868 EMG encoder plus projection head while keeping the pose encoder frozen. The contrastive tem-
 869 perature τ is learnable (initialized to 0.02). All output embeddings are ℓ_2 -normalized. All model
 870 trainings are conducted on $4 \times$ NVIDIA V100 GPUs; end-to-end training of each model takes ap-
 871 proximately 5 hours. CPEP, Q-Former, and EMBridge are all trained for 40 epochs. $N_c = 138$
 872 clusters were computed using K-means from the anchor pose embeddings. The output embedding
 873 size used in linear probing is 256. Batch size is 256 for all models. Increasing batch size (512, 1024)
 874 for CPEP and Q-Former will degrade the performance, but EMBridge’s performance remains robust
 875 as shown in Table 4

876 **Table 4: Impact of batch size on zero-shot classification performance.**

Method	Batch Size 256	Batch Size 512	Batch Size 1024
CPEP	0.481	0.413	0.316
Q-Former	0.498	0.431	0.328
EMBridge (Ours)	0.528	0.526	0.523

883 In zero-shot retrieval, we precompute pose embeddings for the entire corpus and, for each EMG
 884 query, retrieve the top- k neighbors by cosine similarity with $k=10$; the predicted label is the majority
 885 vote of the retrieved labels. For linear probing on *emg2pose* benchmark models, we replace the final
 886 decoding layer with a randomly initialized linear layer for classification, we average the embeddings
 887 at each timepoint as input to the classification layer.

888
 889
 890
 891
 892
 893
 894
 895
 896
 897
 898
 899
 900
 901
 902
 903
 904
 905
 906
 907
 908
 909
 910
 911
 912
 913
 914
 915
 916
 917